Design of A High Single-mode-yield 1.3-µm EMLs with PCG-DFB Lasers and integrated SOA for Future Mobile Applications

Siti Sulikhah
Department of Electronic and Computer Engineering
National Taiwan University of Science and Technology
Taipei 10607, Taiwan
d10602812@mail.ntust.edu.tw

Kai-Chun Ma
Department of Electronic and Computer Engineering
National Taiwan University of Science and Technology
Taipei 10607, Taiwan
m11019003@mail.ntust.edu.tw

San-Liang Lee
Department of Electronic and Computer Engineering
National Taiwan University of Science and Technology
Taipei 10607, Taiwan
sllee@mail.ntust.edu.tw

***Abstract*—EMLs-based partial-corrugated-grating (PCG) DFB-integrated SOA are optimized to achieve a higher output power and a small low-frequency drop (LFD). By selecting a proper SOA length/current, the PCG-EML-integrated SOA could produce >4.77-dB enhancement with 0.39-dB LFD.**

Keywords—electro-absorption modulator, mobile technology, partial grating, optical amplifier, optical communication

I. Introduction

To encounter the huge demand for 5G and the next-generation mobile network technology, the forthcoming optical communication system will require high-speed, high-power, high-reliability, high-stability, robust, compact, and low-cost light sources used in long-haul transmission [1]. Nowadays, the IEEE 802.3ck and 802.3df standards with 1.6TbE supporting 200-Gb/s were authorized, whereas the upcoming 6.4TbE will be projected by 2030 [2-4]. There are several reports on designing semiconductor lasers for these applications, such as long cavity DFB lasers, packaged electro-absorption modulated lasers (EMLs), and EMLs-integrated semiconductor optical amplifiers (SOAs) [5-10]. Although the EMLs have been developed, there is a challenge on how to further improve the light output since the electro-absorption modulator (EAM) has a bias-dependent insertion loss. Moreover, the laser is essentially very sensitive to the influence of residual facet reflection (RFR). Therefore, the EML with a high-tolerance, boosted optical power, and operating speed is required for surpassing the current limitation on the transmission of 100-Gb/wavelength or beyond PAM-4 without sacrificing the power consumption [7].

The SOA-integrated EML is well-known for boosting output power by selecting the driving operations while maintaining good power conversion efficiency (PCE) [11-12]. It becomes an attractive solution for the issues mentioned above, which can independently amplify the output from the EAM with great efficiency [13-14]. A clear waveform after long transmission could be managed as modulated optical output is enhanced. Hence, modulated light output power with the same power consumption is feasible to double. By taking these benefits, a SOA-integrated EML can contribute to extending the number of branches of passive optical networks (PONs) in the optical access system. Furthermore, by taking into account cost and packaging yield, an optical line terminal (OLT) transmitter of a 50-Gb/s-based optical network unit (ONU) will demand an EML-SOA [15]. In addition, the SOA-integrated EML can govern an average output power of about 9-dBm over the -40ºC to 85ºC temperature range [16].

In our prior works, a better single-mode-yield (SMY) and a higher tolerance to RFR effects can be performed by EMLs with partial corrugated grating type DFB laser (PCG-EML) against the original uniform grating structure (UG-EML) [17]. Both experiments and simulation using VPIcomponentMaker Photonics Circuits Tool (i.e., efficient techniques and professional design function for optoelectronic devices and complex photonic integrated structures like EML) have been conducted to affirm the resultant low-frequency drop (LFD), which can be a key indicator to screen out the EMLs in high-speed optical transceivers since it is bias-dependent and laser-structure dependent [18-20]. In this work, we will investigate the static and dynamic performances of the integration of PCG-EML with SOA (e.g., EAM absorption, longitudinal power distribution, light-output, side-mode suppression ratio (SMSR), wavelength shift, intensity modulation (IM) response, relative intensity noise (RIN) characteristic, and undershoot/overshoot at 56-Gb/s NRZ signal) with a variation of SOA lengths and its bias currents. These extensive analyses would be significantly beneficial for developing an advanced light source realizing 5G and beyond 5G networks.

II. Device Structure and Characteristics

Fig. 1 depicts the schematic views of PCG-EML with integrated SOA, which consists of an uncorrugated waveguide near the HR rear facet, a corrugated grating (L_g = 175-µm) close to the EAM facet, and SOA section (AR coating at front facet). The DFB section and EAM lengths are set by 300-µm and 100-µm, while the respective lengths of SOA are 100, 200, and 300-µm, accordingly. The DFB laser is biased with a DC current of 70-mA, whereas the bias ratio (r) of SOA and DFB section is 0.5, 1, and 1.5, respectively.

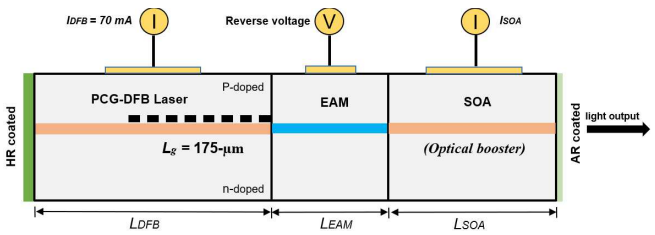

Fig. 1. Schematic views of PCG-EML with integrated SOA.

The EAM is modulated with a reverse bias voltage of -1 V and 0.5 V voltage swing. Here, the input power is allocated to each section independently. The SOA and DFB laser has the same MQW structure to reduce the complexity of the design process as that of the conventional EML. Table 1 lists the key laser parameter used in analyzing the PCG-EML-integrated SOA. The laser gain material involves a typical MQW

structure operating at 1310-nm wavelength. The modulator is modulated by 56-GB/s PRBS-NRZ pattern.

TABLE I. LIST OF DEVICE PARAMETERS

Parameter	Value	Parameter	Value
Laser length	300 μm	Coupling coeff.	5000 m^{-1}
Modulator length	100 μm	Group index	3.73
Active region width	1.8 μm	Peak absorption frequency	234.025 THz
Active region thickness	0.03 μm	Transparent carrier density	$1.5x10^{24}$ m^{-3}
Optical confinement factor	0.075	Gain compress. factor	$2.5x10^{-23}$ m^3
Internal loss	25 cm^{-1}	α parameter	3

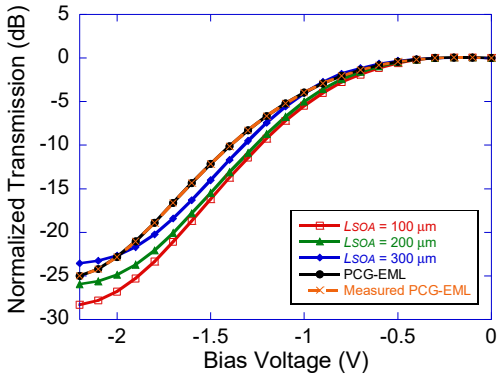

Fig. 2. Comparison of measured EAM absorption of PCG-EML and its integration with SOA.

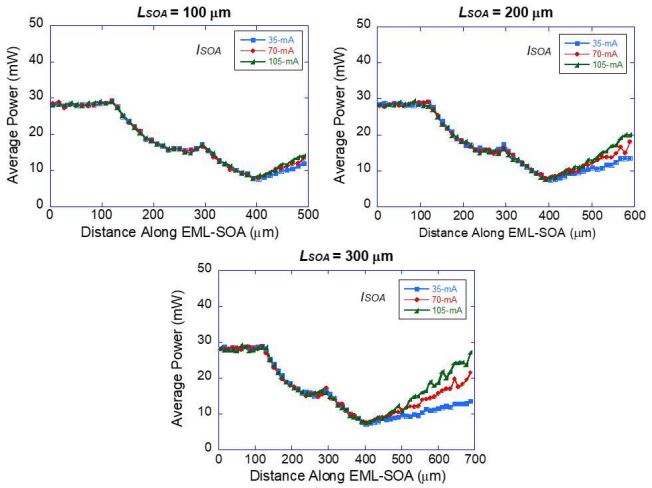

Fig. 3. Longitudinal total power distribution for SOA-integrated PCG-EML with different SOA lengths and SOA currents at $R_f = 0$.

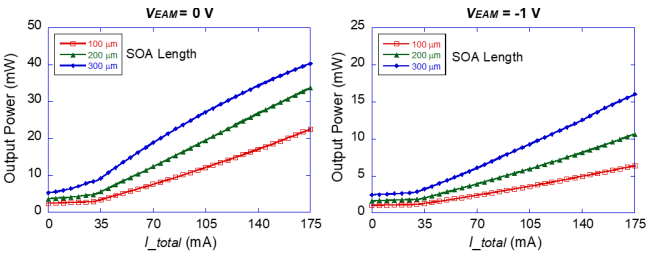

Fig. 4. L-I curves of PCG-EML with integrated SOA with different SOA lengths when the EAM is ON and OFF, respectively ($r = 1.5$).

The measured EAM absorption of PCG-EML (dashed line) and comparison of normalized transmission curves for PCG-EML-integrated SOA with different SOA lengths is shown in Fig. 2, which resulted in a static extinction ratio (SER) of 8.01-dB under facet reflectivity ($R_f = 0$) at I_{SOA} = 105-mA. Fig. 3 shows the longitudinal total power distribution for the HR phase of 30º with SOA lengths and SOA currents variation. To demonstrate the light-output power (L-I) curve of PCG-EML-integrated SOA, both currents of DFB and SOA sections are varied at the same time, which is applied when the EAM is ON (V_{EAM} = -1 V) and OFF (V_{EAM} = 0 V), correspondingly. The light output power of SOA-integrated PCG-EML is increased by up to 4.77-dB, compared with that of the PCG-EML, as in Fig. 4. The light output is gradually enhanced as the L_{SOA} is increased (optical booster), so the efficiency also becomes larger as the SOA lengths become longer. Noticing that insufficient gain may occur if the SOA length is too short, but the gain saturation deteriorates the signal quality and non-linearity by resonance behavior when the SOA section is too long. Based on our observation, only a tiny change appears when a different R_f is set. A reduced optical power can be seen for V_{EAM} = -1 V as a large insertion loss arises from EAM.

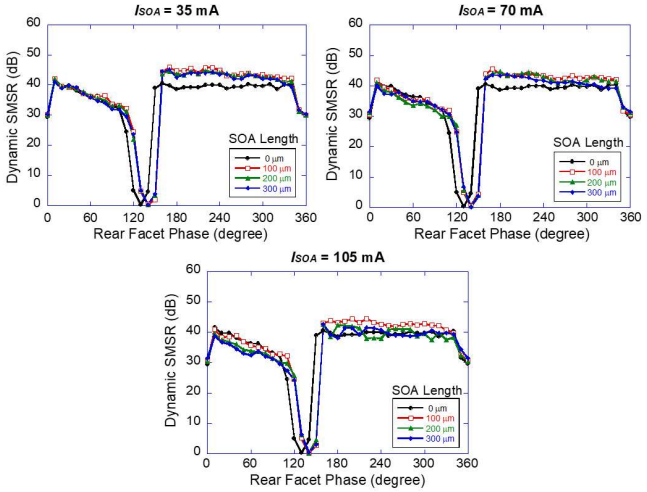

Fig. 5. Simulated dynamic SMSR for PCG-EML with integrated SOA versus SOA length and SOA current at $R_f = 0$.

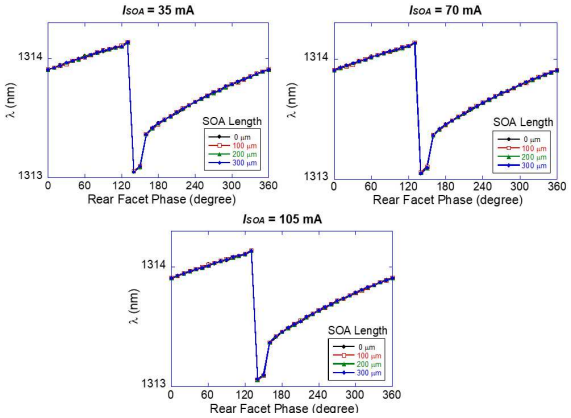

Fig. 6. Wavelength changes under dynamic conditions for PCG-EML with integrated SOA with different SOA lengths and SOA current at $R_f = 0$.

III. DYNAMIC RESPONSES

The simulated dynamic SMSR under the rear facet phase variation from 0 to 2π at $R_f = 0$ is depicted in Fig. 5. The SMY accounts for those phases having SMSR >35-dB for both static and dynamic conditions. In general, PCG-EML with integrated SOA could provide dynamic SMY as high as 72.97% with an average dynamic SMSR exceeding 37.87-dB. From Fig. 6, the wavelength fluctuation Δλ is around 1.08-nm as the facet phase changes. Fig. 7 displays the RIN

characteristics of the original PCG-EML and PCG-EML with integrated SOA, where the latter has a slightly higher noise.

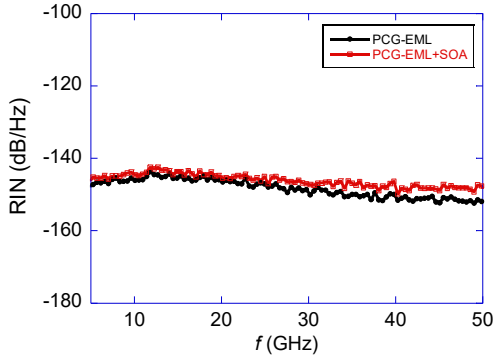

Fig. 7. Typical RIN characteristics for PCG-EML and PCG-EML-integrated SOA (HR phase = 10º).

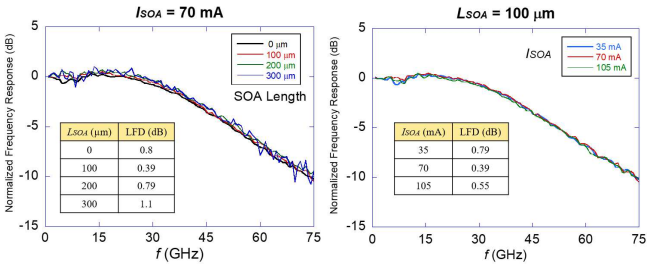

L_{SOA} (µm)	LFD (dB)
0	0.8
100	0.39
200	0.79
300	1.1

I_{SOA} (mA)	LFD (dB)
35	0.79
70	0.39
105	0.55

Fig. 8. Simulated IM responses for PCG-EML and PCG-EML-integrated SOA at $R_f = 10^{-3}$ and HR phase = 30º.

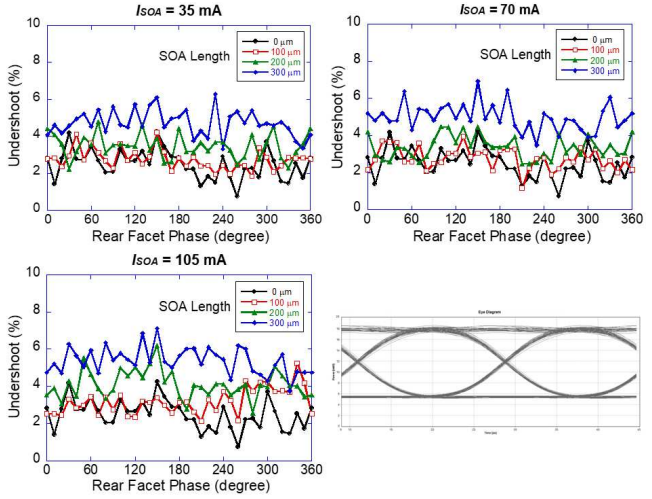

Fig. 9. Simulated undershoot for PCG-EML-integrated SOA with different SOA lengths and SOA currents at $R_f = 0$.

Fig. 8 compares the simulated intensity modulation responses for PCG-EML and PCG-EML with integrated SOA for $R_f = 10^{-3}$ and HR phase = 30º. The simulation suggests that the proposed structure could produce a lower LFD of 0.39-dB (L_{SOA} = 100-µm and I_{SOA} = 70 mA) compared to the original PCG-EML. There is a trade-off in selecting the length and bias current of SOA to get a good IM response. The SOA-integrated PCG-EML can provide an improved static/dynamic performance with a lower LFD. It discloses the influence of the RFR on the EML caused by carrier density fluctuation. Consequently, the immunity to RFR evidently enhances the PCG-EML with integrated SOA. Under 56-Gb/s NRZ signal, it could have a quite small undershoot (<5.29%) and overshoot (<9.31%), assuming there is no RFR at the SOA side, as shown in Fig. 9 and Fig. 10 respectively.

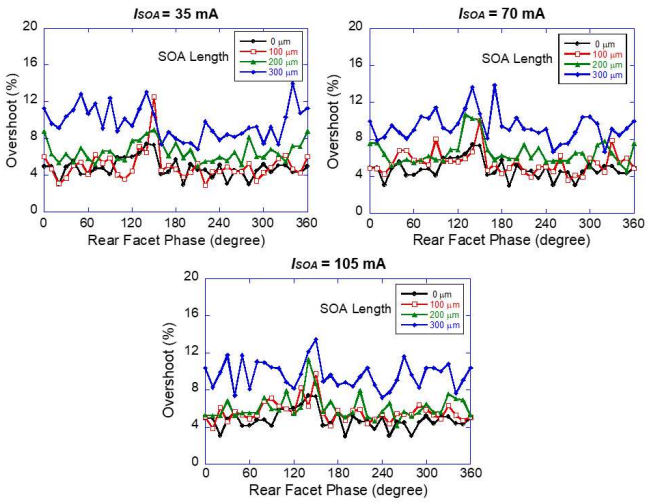

Fig. 10. Simulated overshoot for PCG-EML-integrated SOA with different SOA lengths and SOA currents at $R_f = 0$.

IV. Conclusion

In this report, we analyzed the performance of adding a SOA after PCG-EML (L_g = 175-µm) for both static and dynamic conditions. The simulation results propose an enhanced output power >4.77-dB with superior extinction characteristics (dynamic SMY of >67.57%). We found that PCG-EML-integrated SOA has a good RIN characteristic, stable operation, an appropriate undershoot/overshoot, and a smaller LFD compared to the original PCG-EML, which results from a better resistance to RFR. Therefore, an advanced PCG-EML-integrated SOA can be a strong candidate for the light source of 200-Gb/s against those of conventional EML.

Acknowledgment

The work was supported in part by the National Science and Technology Council (NSTC) of Taiwan, under the grant number NSTC 109-2221-E-011-153-MY3.

References

[1] J. S. Zou, *et al*., J. Opt. Comm. Netw., vol. 12, pp. D86-D-98, Oct. 2020.

[2] J. D. Ambrosia, "The case for 1.6 terabit ethernet," IEEE 802.3 Beyond 400 Gb/s Ethernet Study Group Meeting, 2021, pp. 1-18.

[3] D. Lewis, Ethernet Alliance. TEF 2021: The Road Ahead Next Generation Optical Interfaces, 2021, pp. 1-20.

[4] C. Lam, *et al*., IEEE 802.2 NEA Meeting, 2020, pp. 1-20.

[5] O. Ozolins, *et al*., J. Lightw. Technol., vol. 35, pp. 1174-1179, 2017.

[6] A. Abbasi, *et al*., IEEE JSTQE, vol. 23, Nov.-Dec. 2017, Art. no. 1501307.

[7] T. Shindo, *et al*., NTT Tech. Review, vol. 17, pp. 42-49, Oct. 2019.

[8] S. Yamauchi, *et al*., OFC, San Diego, USA, 2021, Paper Tu1D.1.

[9] H. Grant, *et al*., SPIE OPTO, San Francisco, USA, 2022, Paper PC12004.

[10] S. Yokokawa, *et al*., OFC, San Diego, USA, 2022, Paper M4D.3.

[11] D. Inoue, *et al*., OFC, San Diego, USA, 2023, Paper M4C.4.

[12] M. A. D. Theurer, PhD dissertation, Technische Universitat Berlin, 2021.

[13] W. Kobayashi, *et al*., J. Lightw. Technol., vol. 28, pp. 164-171, 2010.

[14] W. Kobayashi, *et al*., ECOC, Cannes, France, 2014, Paper Mo.4.4.5.

[15] E. Harstead, *et al*., J. Opt. Comm. Netw., vol. 12, pp. D17-D26, 2020.

[16] V. Houtsma, *et al*.,. Opt. Comm. Netw., vol. 13, pp. A44-A55, 2021.

[17] S. Sulikhah, *et al*., OECC, Taipei, Taiwan, 2020, pp. 1-3.

[18] V. Photonics, "VPI component maker photonic circuit," Available: https://www.vpiphotonics.com/Tools/ PhotonicCircuits/.

[19] S. Sulikhah, *et al*., PHOTOPTICS, 2022, pp. 1-7.

[20] S. Sulikhah, *et al*., IEEE Photon. J., vol. 14, Apr. 2022, Art. no. 1515409.